

General constraints on sources of high energy cosmic rays. Updated Hillas diagrams.

Simon Sotirov

Institute for Nuclear Research of the Russian Academy of Sciences, 60th October Anniversary Prospect 7a, Moscow 117312, Russia

E-mail: sotirov.sa19@physics.msu.ru

While the precise origins of high-energy cosmic rays remain elusive, various constraints can be placed on their possible sources. One such approach involves the Hillas diagram, a graphical representation that delineates the range of geometric sizes and magnetic fields of plausible astrophysical accelerators. Previous iterations of this diagram considered geometric criteria and radiation losses to establish these boundaries. In this study, we expand on the Hillas diagram for protons, incorporating the energy losses associated with photohadronic and Bethe-Heitler processes. This updated diagram links the allowable regions to the source's electromagnetic luminosity, resulting in the most stringent constraints for compact, bright sources like the central regions of active galactic nuclei.

*International Conference on Particle Physics and Cosmology (ICPPCRubakov2023)
02-07, October 2023
Yerevan, Armenia*

INTRODUCTION

Despite extensive research on high-energy cosmic rays and astrophysical neutrinos, their exact sources remain uncertain [1, 2]. To narrow down the search for these elusive sources, it's crucial to establish constraints on their physical properties. A well-known constraint is the Hillas criterion [3], which dictates that particles must remain confined within the accelerator region until they acquire the requisite energy. This confinement is typically attributed to the interplay between the magnetic field, which holds the particle, and the electric field, which accelerates it.

A second constraint stems from the energy loss associated with a charged particle's acceleration. This energy loss impedes further acceleration and must be considered when evaluating potential sources of ultra-high-energy particles. These constraints can be visualized using a diagram that plots magnetic field strength against source size, known as the Hillas diagram. Lines representing the Hillas criterion delineate the permissible range of parameters for astrophysical sources capable of accelerating particles to the corresponding energies. Detailed calculations and diagrams are presented in various studies.

This study aims to further restrict the pool of potential sources for cosmic rays and, consequently, high-energy neutrinos. To achieve this, the authors incorporate the energy loss experienced by protons due to interactions with source photons. Localized photon concentrations, particularly at lower energies, influence this interaction. The main contributions to the photohadronic cross section are considered to be Δ^+ production and multipion production. Additionally, the Bethe-Heitler process is taken into account. Energy loss calculations for interactions assume diffuse acceleration (e.g., shock waves [4]) of protons. For specific assumptions about radiation fields, these losses are presented in the Hillas diagram [5–8], further limiting the region of potential sources capable of accelerating protons to the specified energies.

PROTON ENERGY LOSSES

radiation losses

Radiation losses can be divided into two types: synchrotron and curvature losses [9]. In the ultrarelativistic regime, curvature losses are generally insignificant. For any typical field configuration, synchrotron losses are the dominant factor. However, in a specific scenario where the particle's velocity, magnetic field B , and electric field are parallel, synchrotron losses vanish and curvature losses take over. The synchrotron losses for a proton moving in an astrophysical source with a magnetic field B are expressed as [6]:

$$-\frac{dE_{\text{rad}}}{dt} = \frac{2}{3} \frac{\alpha^2}{m_p^4} E^2 B^2 = 1.5 \cdot 10^{-29} \times \left(\frac{E}{\text{eV}}\right)^2 \left(\frac{B}{\text{G}}\right)^2 \text{ eV/s}, \quad (1)$$

where m_p is a proton mass, α - is the fine structure, E - proton energy.

interaction losses

The most important contribution to the total cross section is the creation and subsequent decay of Δ^+ [10, 11]:

$$p + \gamma \rightarrow \Delta^+ \rightarrow \begin{cases} n + \pi^+ \\ p + \pi^0. \end{cases} \quad (2)$$

The next important contribution is multipion production. The total $p\gamma$ interaction cross section $\sigma_{p\gamma}$ can be estimated as the sum of these two channels, as a result of which an analytical approximation can be used [10]:

$$\sigma_{p\gamma}(\epsilon_r)K_{p\gamma}(\epsilon_r) = 70H(\epsilon_r - \epsilon_{\text{thr}}) \mu\text{b}, \quad (3)$$

where $\epsilon_r = \gamma_p \epsilon (1 - \beta_p \mu)$ is energy invariant of the interaction, where $\mu = \cos \theta$, θ is the angle between the colliding proton and photon momenta. $\gamma_p = (1 - \beta_p^2)^{-1/2}$ is proton Lorentz factor, ϵ is energy of the target photons in units of an electron mass m_e , $K_{p\gamma}$ is the inelasticity of the collision, $\epsilon_{\text{thr}} = 390$ and H is the Heaviside step function.

The inverse of the photohadronic energy-loss timescale for high energy protons is given by the standard expression (in the particle physics $c = 1$ units):

$$t_{\gamma p}^{-1} \cong \frac{1}{2\gamma_p^2} \int_0^\infty \frac{n_{\text{ph}}(\epsilon)}{\epsilon^2} d\epsilon \int_0^{2\gamma_p \epsilon} \epsilon_r \sigma_{p\gamma}(\epsilon_r) K_{p\gamma}(\epsilon_r) d\epsilon_r, \quad (4)$$

where $n_{\text{ph}}(\epsilon)$ is a spectral number density of source photons.

First, consider the case of a power-law spectrum $n_{\text{ph}} = \beta \epsilon^{-\alpha}$. It is assumed spherical source with radius R . By using (3) and performing the integral over the interval from ω to $+\infty$ (or from ω to Ω in the case of a hard spectrum) in (4) the expression for the proton energy losses due to $p\gamma$ interactions can be obtained in the form:

$$\frac{dE}{dt} = \begin{cases} \left(\frac{\alpha-2}{\alpha^2-1} \cdot 10^{-89} \times \left(\frac{E}{\text{eV}} \right)^2 \left(\frac{R}{\text{kpc}} \right)^{-2} \left(\frac{L_{\geq \omega}}{\text{eV/s}} \right) \right) \text{eV/s}, & \alpha > 2 \\ 5 \cdot 10^{-90} \left(\ln \frac{\Omega}{\omega} \right)^{-1} \times \left(\frac{E}{\text{eV}} \right)^2 \left(\frac{R}{\text{kpc}} \right)^{-2} \left(\frac{\tilde{L}_{\geq \omega}}{\text{eV/s}} \right) \text{eV/s}, & \alpha = 2 \\ \left(\frac{2-\alpha}{\alpha^2-1} 6^\alpha \cdot 10^{-12\alpha-68} \Omega^{\alpha-2} \times \left(\frac{E}{\text{eV}} \right)^\alpha \left(\frac{R}{\text{kpc}} \right)^{-2} \left(\frac{\tilde{L}_{\geq \omega}}{\text{eV/s}} \right) \right) \text{eV/s}, & \alpha < 2 \end{cases} \quad (5)$$

where β expressed in terms of $L_{\geq \omega}$ (for $\alpha > 2$) or $\tilde{L}_{\geq \omega}$ (for $\alpha \leq 2$), where $L_{\geq \omega}$ is the source bolometric luminosity at a photon energy greater than $\omega = m_e \epsilon_{\text{thr}} / 2\gamma_p$ and $\tilde{L}_{\geq \omega}$ is the same but for photon energies greater than ω and less than Ω . Where Ω is the high energy cutoff of a source spectrum.

However in addition to photohadronic processes there is Bethe-Heitler interactions $p + \gamma \rightarrow p + e^- + e^+$ [12–14]. Expressions for energy losses can be written similarly for them (power-law case):

$$\frac{dE}{dt} = \begin{cases} 10^{-89}(\alpha - 2)\epsilon_{\text{thr}}^{\alpha-2}I(2) \times \left(\frac{E}{\text{eV}}\right)^2 \left(\frac{R}{\text{kpc}}\right)^{-2} \left(\frac{L_{\geq\omega}}{\text{eV/s}}\right) \text{eV/s}, & \alpha > 2, \\ 2 \cdot 10^{-89} \left(\ln \frac{\Omega}{\omega}\right)^{-1} I(2) \times \left(\frac{E}{\text{eV}}\right)^2 \left(\frac{R}{\text{kpc}}\right)^{-2} \left(\frac{\tilde{L}_{\geq\omega}}{\text{eV/s}}\right) \text{eV/s}, & \alpha = 2, \\ 10^{-71-9\alpha}(2 - \alpha) \left(\frac{\Omega}{m_e}\right)^{\alpha-2} I(\alpha) \times \left(\frac{E}{\text{eV}}\right)^\alpha \left(\frac{R}{\text{kpc}}\right)^{-2} \left(\frac{\tilde{L}_{\geq\omega}}{\text{eV/s}}\right) \text{eV/s}, & \alpha < 2, \end{cases} \quad (6)$$

where

$$I(\alpha) = \int_2^\infty \frac{\epsilon^{-\alpha}\varphi(\epsilon)}{\epsilon^2} d\epsilon \quad (7)$$

φ is the fitting function with the relative error $< 1.5 \times 10^{-3}$ [15].

ACCELERATION MODEL

Similar to the [6], this study focuses on the diffuse mechanism acceleration model. In the most common scenarios, particles gain energy within the accelerator by repeatedly interacting with shocks. Since this model assumes a disordered field configuration, energy losses and radiation are solely attributed to synchrotron radiation. Consider the trajectory of a particle traversing a magnetized source medium. The particle acquires energy through repeated scattering on a shock wave. Afterwards, it follows an approximately Larmor orbit over extended distances, losing energy through radiation and interactions with low-energy photons in the medium until encountering the next shock wave. This process continues cyclically. As we will observe, the particle's maximum energy upon leaving the source is weakly dependent on the energy gained directly at the shock front. Instead, it is primarily determined by energy losses.

Let's examine a particle with an initial energy (at the shock wave front) traveling through a region of a specified size filled with a magnetic field and exiting the source. As the particle moves through the medium, its energy diminishes due to interactions and radiation processes.

In addition to considering energy losses, it is also crucial to adhere to the geometric criterion, also known as the Hillas criterion. This criterion stipulates that a particle's Larmor radius must not exceed the extent of the accelerator. If this constraint is violated, the particle will escape the accelerator before it has gained the required energy. This criterion can be expressed mathematically as an inequality:

$$E \leq 9.25 \cdot 10^{23} \times \left(\frac{B}{\text{G}}\right) \left(\frac{R}{\text{kpc}}\right) \text{eV}. \quad (8)$$

All these constraints for the diffuse acceleration mode are presented graphically in Fig. 1.

IMPLICATIONS

By leveraging the findings of this study, we have updated the Hillas diagram, incorporating constraints related to proton-photon interactions, including photohadronic and Bethe-Heitler interactions. This expansion introduces an additional parameter – luminosity – to the diagram. As

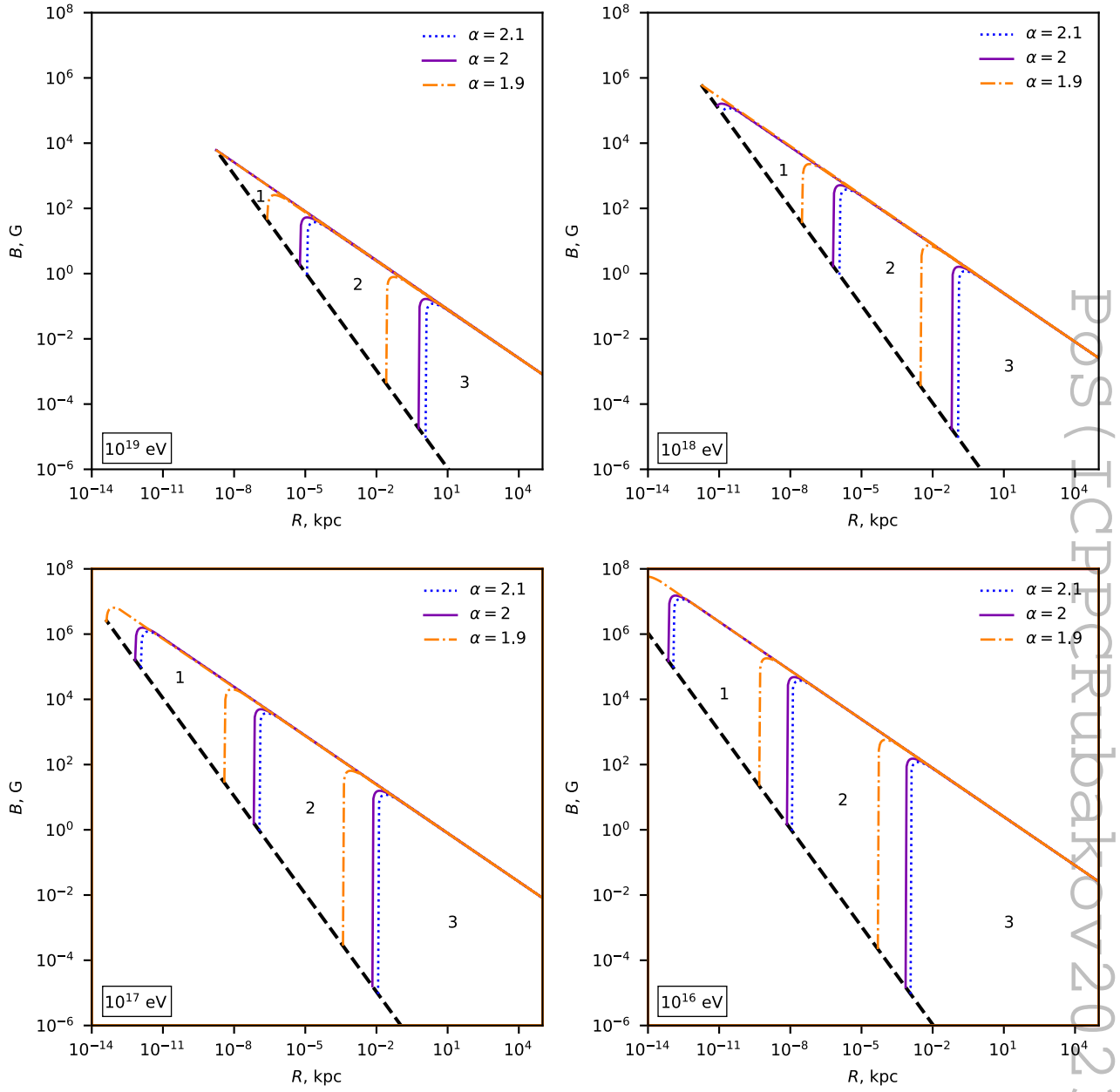


Figure 1: Magnetic field - source size diagram for proton acceleration for power-law radiation field. The black dashed line is the geometric criterion. The dotted blue lines, solid magenta lines and dot-dashed lines are the constraints associated with losses due to radiation in a magnetic field and due to interaction with source photons for $\alpha = 2.1$, $\alpha = 2$ and $\alpha = 1.9$ respectively. The lines limit the range of parameters that the source can have in order to accelerate protons to a given energy. In this case, each graph corresponds to a certain energy: 10^{16} eV, 10^{17} eV, 10^{18} eV, 10^{19} eV. In the case of 10^{16} eV, the region 1+2+3 corresponds to the region of parameters (R,B) that a source with luminosity $L_{\geq 0.9 \text{ keV}} = 10^{38} \text{ erg s}^{-1}$ can have, in order to accelerate protons up to 10^{16} eV. Region 2+3 is similar, but for luminosity $L_{\geq 0.9 \text{ keV}} = 10^{43} \text{ erg s}^{-1}$. Region 3 corresponds to luminosity $L_{\geq 0.9 \text{ keV}} = 10^{48} \text{ erg s}^{-1}$. In the case of 10^{17} eV 1+2+3 corresponds to $L_{\geq 90 \text{ eV}} = 10^{38} \text{ erg s}^{-1}$, 2+3 corresponds to $L_{\geq 90 \text{ eV}} = 10^{43} \text{ erg s}^{-1}$, Region 3 for $L_{\geq 90 \text{ eV}} = 10^{48} \text{ erg s}^{-1}$. In the case of 10^{18} eV 1+2+3 corresponds to $L_{\geq 9 \text{ eV}} = 10^{38} \text{ erg s}^{-1}$, 2+3 corresponds to $L_{\geq 9 \text{ eV}} = 10^{43} \text{ erg s}^{-1}$, Region 3 for $L_{\geq 9 \text{ eV}} = 10^{48} \text{ erg s}^{-1}$. And finally, in the case of 10^{19} eV 1+2+3 corresponds to $L_{\geq 0.9 \text{ eV}} = 10^{38} \text{ erg s}^{-1}$, 2+3 corresponds to $L_{\geq 0.9 \text{ eV}} = 10^{43} \text{ erg s}^{-1}$, Region 3 for $L_{\geq 0.9 \text{ eV}} = 10^{48} \text{ erg s}^{-1}$. For spectra with $\alpha = 2$ and $\alpha = 1.9$ it is assumed $\Omega = 10^{15} \text{ eV}$.

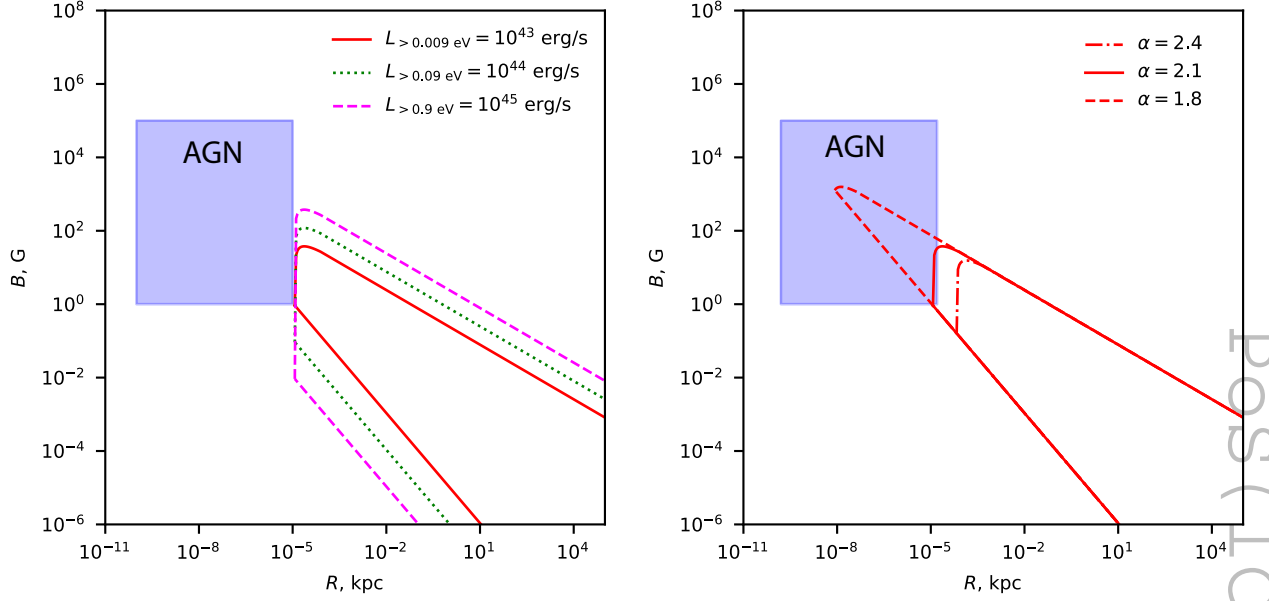


Figure 2: Magnetic field B - source size R diagrams. The blue rectangle is the area of parameters (R, B) that central regions of AGNs can have. Left : the solid red line limits the range of parameters that sources with luminosities $L_{\geq 0.009 \text{ keV}} = 10^{43} \text{ erg s}^{-1}$ can have in order to accelerate protons up to 10^{19} eV . The dotted green line limits the range of parameters that sources with luminosities $L_{\geq 0.09 \text{ keV}} = 10^{44} \text{ erg s}^{-1}$ can have in order to accelerate protons up to 10^{18} eV . The magenta line limits the range of parameters that sources with luminosities $L_{\geq 0.9 \text{ keV}} = 10^{45} \text{ erg s}^{-1}$ can have in order to accelerate protons up to 10^{17} eV . Right : lines for different spectral indices α for 10^{19} eV and $L_{\geq 0.009 \text{ keV}} = 10^{43} \text{ erg s}^{-1}$. For spectrum with $\alpha = 1.8$ it is assumed $\Omega = 10^{15} \text{ eV}$.

illustrated in the figure, lower luminosity corresponds to a broader range of parameters within which particle acceleration to a given energy can occur. This observation enables us to place constraints on compact, high-luminosity sources, such as the central regions of the nuclei of active galaxies (AGNs).

The location of the central regions of the AGNs on the Hillas diagram can be derived with simple estimations [5]:

$$R \sim 5R_s \approx 5 \times 10^{-8} \frac{M_{\text{BH}}}{10^8 M_{\odot}} \text{ kpc}, \quad (9)$$

where M_{BH} is the black hole mass, R_s - gravitational radius. M_{BH} varies from $10^6 M_{\odot}$ for ordinary galaxies to $10^{10} M_{\odot}$ for powerful radio galaxies and quasars.

The magnetic field near the black hole's horizon B_{BH} is highly dependent on the black hole's mass. A conservative estimate is obtained, for example, in [16]:

$$B_{\text{BH}} = 10^8 \left(\frac{M_{\text{BH}}}{M_{\odot}} \right)^{-0.5} \text{ G}. \quad (10)$$

Using (9) and (10), it is possible to graphically limit the region of parameters of the central regions of AGNs on the diagram, which is shown in Fig. 2. It can be seen that for some α the central

regions of AGNs with luminosities $L_{\geq 0.009 \text{ eV}}$ greater than $10^{43} \text{ erg s}^{-1}$ cannot accelerate protons up to 10^{19} eV and higher in the diffuse acceleration mode and so on.

Throughout this work, we carry out calculations in the reference frame of the source photon (where the photons are isotropic), and $L_{\geq \omega}$ (or $\tilde{L}_{\geq \omega}$) denotes the total 4π luminosity, which is a Lorentz invariant. For particular sources, especially for relativistic jets of active galactic nuclei, the Doppler enhancement of the observable flux should be taken into account when using observational data to estimate $L_{\geq \omega}$ (or $\tilde{L}_{\geq \omega}$), see e.g. [10].

thermal radiation case

It's also valuable to examine the thermal spectrum, which can effectively represent the central regions of AGNs with temperatures ranging from 10 to 100 eV [16]. AGNs are potential sources of astrophysical neutrinos. At the core of an AGN, a supermassive black hole (SMBH) is encircled by an accretion disk that emits thermal radiation. This study assumes (as per previous research) that proton acceleration occurs in the SMBH's vicinity and then travels along two jets perpendicular to the accretion disk [17, 18]. As protons propagate, they interact with low-energy photons emanating from the accretion disk. The spectral number density along the axis from the disk is taken as

$$n_{\text{ph}} = x^2 \frac{2\pi}{\lambda_C^3} \frac{\epsilon^2}{\exp(\epsilon/\Theta) - 1}, \quad (11)$$

where λ_C^3 is the electron Compton wavelength, $\Theta = T/m_e$ is the dimensionless temperature of the radiation field, $x = R_{\text{AD}}/R_{\text{dist}}$. R_{AD} is the typical accretion disc size which can be fitted as [19]:

$$R_{\text{AD}} = 10^{15} \left(\frac{M}{10^8 M_{\odot}} \right) \text{cm}. \quad (12)$$

Energy losses can be obtained using (3), (4):

$$\begin{aligned} \frac{dE}{dt} = & -Q_1 \Theta^3 \kappa(E) \left(\frac{E}{\text{eV}} \right) - Q_2 \xi(E) \left(\frac{E}{\text{eV}} \right)^{-2} \\ & - D \left(\frac{E}{\text{eV}} \right)^2 \left(\frac{B}{\text{G}} \right)^2 \text{ eV/s}, \end{aligned} \quad (13)$$

where $Q_1 = 3.82 \cdot 10^{12}$, $Q_2 = 6.5 \cdot 10^{38}$, $D = 1.5 \cdot 10^{-29}$

$$\kappa(E) = \int_{\tilde{\omega}}^{\infty} dy \frac{y^2 - \tilde{\omega}^2}{e^y - 1}, \quad (14)$$

$$\xi(E) = \int_2^{\infty} d\epsilon \frac{\varphi(\epsilon)}{\exp(\epsilon m_p / 2E\Theta) - 1}, \quad (15)$$

and $\tilde{\omega} = m_e \epsilon_{\text{thr}} / 2\Theta \gamma_p$.

Consider a proton propagating in a jet. Let it interact with a shock at distance R_{dist} receive energy E_0 and leave the jet after passing distance R . Similarly, as was done for the power law spectrum in the limit $E_0 \rightarrow \infty$ we obtain Hillas diagram Fig. 3. The lower the temperature, the larger the allowable area on the Hillas diagram, since with decreasing temperature the photon density (11) decreases and the proton loses less energy for interaction. Diagrams for various temperatures

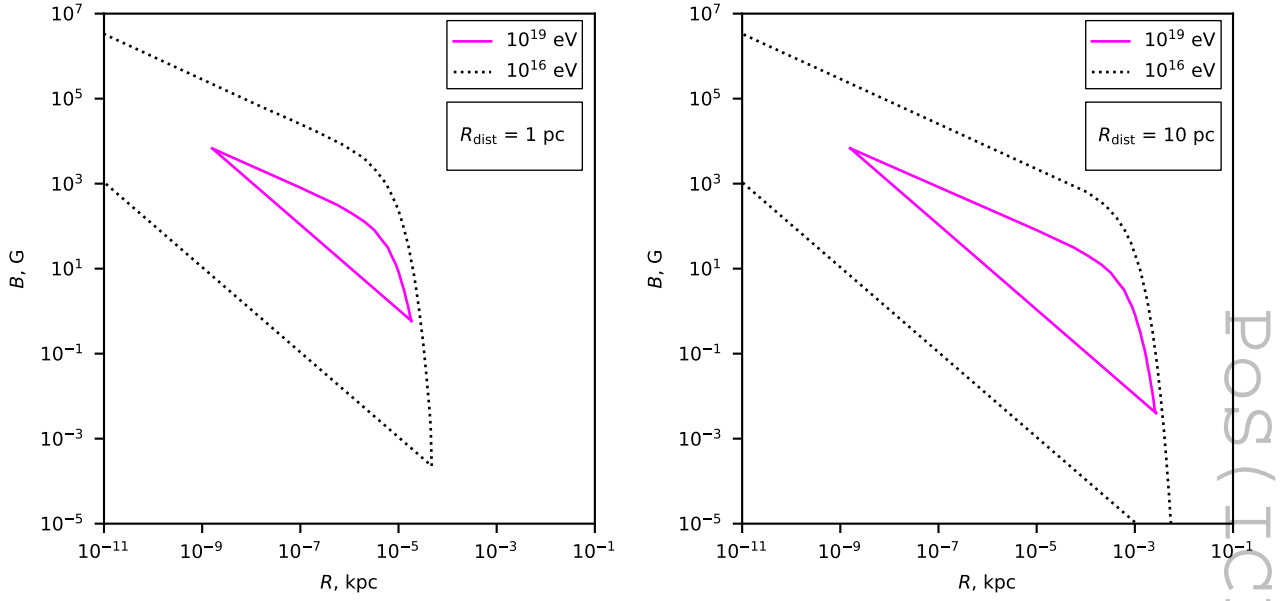


Figure 3: Magnetic field-size diagram. The magenta solid line limits the range of parameters at which the proton accelerated by a shock at the distance R_{dist} from accretion disc can leave accelerator with energy 10^{19} eV. The same for the black dotted line for 10^{16} eV (see figure). It is assumed this that the SMBH has mass $10^8 M_{\odot}$ and accretion disc has temperature ~ 100 eV.

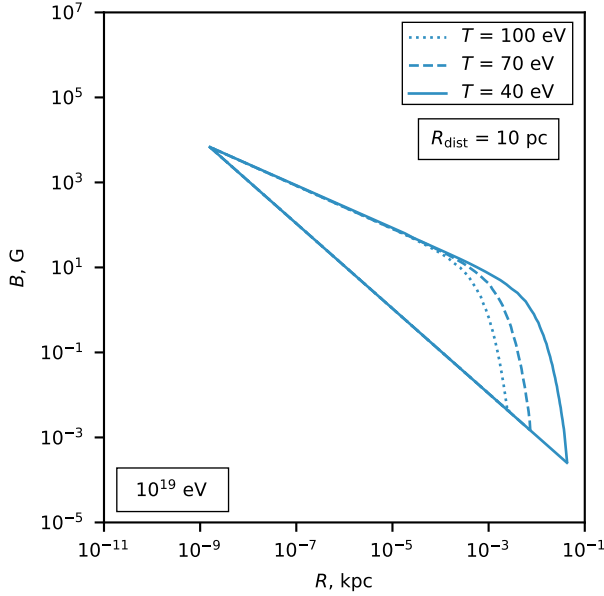


Figure 4: Magnetic field-size diagram. The blue lines limits the range of parameters at which the proton accelerated by a shock at the distance $R_{\text{dist}} = 10$ pc from accretion disc can leave accelerator with energy 10^{19} eV for different temperatures 40 eV, 70 eV, 100 eV. It is assumed this that the SMBH has mass $10^8 M_{\odot}$.

are shown in Fig. 4 In particular for energy 10^{19} eV, temperature 2.7 K and $x = 1$ the standard GZK cutoff ~ 50 Mpc can be turned out.

It should be noted that all these restrictions are made on the assumption that the photon distribution is described by a power-law spectrum and diffuse acceleration mode is assumed. Also as can be seen from the energy loss expressions in the case of a hard spectrum ($\alpha \leq 2$), the diagrams become sensitive to the high-energy cutoff Ω .

CONCLUSIONS

This research expands the Hillas diagram by incorporating a new constraint related to proton-photon interactions. This modification shrinks the allowable parameter space and introduces a parametric dependence of the region's size on luminosity or temperature. The revised diagram highlights the limitations of compact and luminous sources, particularly those found in the central regions of active galactic nuclei (AGNs). Under the assumption of a power-law radiation field and a diffuse acceleration mechanism, a class of AGNs was identified that cannot accelerate protons to energies of 10^{19} eV, 10^{18} eV, or 10^{17} eV. Additionally, the diagram significantly narrows down the search area for high-energy proton accelerators in AGNs with a thermal radiation field. Moreover, the diagram accounts for the interconnected nature of the size, magnetic field, and luminosity of AGN central regions, providing an additional layer of constraints. The paper provides the necessary formulas for constructing the diagram, allowing readers to customize it for their specific needs, such as evaluating the feasibility of proton acceleration within a source with a given luminosity.

References

- [1] A. Palladino, M. Spurio, F. Vissani, Neutrino Telescopes and High-Energy Cosmic Neutrinos, *Universe* 6 (2) (2020) 30. [arXiv:2009.01919](https://arxiv.org/abs/2009.01919), [doi:10.3390/universe6020030](https://doi.org/10.3390/universe6020030).
- [2] M. Kachelriess, D. V. Semikoz, Cosmic Ray Models, *Prog. Part. Nucl. Phys.* 109 (2019) 103710. [arXiv:1904.08160](https://arxiv.org/abs/1904.08160), [doi:10.1016/j.pnpnp.2019.07.002](https://doi.org/10.1016/j.pnpnp.2019.07.002).
- [3] A. M. Hillas, The Origin of Ultrahigh-Energy Cosmic Rays, *Ann. Rev. Astron. Astrophys.* 22 (1984) 425–444. [doi:10.1146/annurev.aa.22.090184.002233](https://doi.org/10.1146/annurev.aa.22.090184.002233).
- [4] F. M. Rieger, P. Duffy, Shear acceleration in relativistic astrophysical jets, *Astrophys. J.* 617 (2004) 155–161. [arXiv:astro-ph/0410269](https://arxiv.org/abs/astro-ph/0410269), [doi:10.1086/425167](https://doi.org/10.1086/425167).
- [5] K. V. Ptitsyna, S. V. Troitsky, Physical conditions in potential sources of ultra-high-energy cosmic rays. I. Updated Hillas plot and radiation-loss constraints, *Phys. Usp.* 53 (2010) 691–701. [arXiv:0808.0367](https://arxiv.org/abs/0808.0367), [doi:10.3367/UFNe.0180.201007c.0723](https://doi.org/10.3367/UFNe.0180.201007c.0723).
- [6] M. V. Medvedev, A Constraint on electromagnetic acceleration of highest energy cosmic rays, *Phys. Rev. E* 67 (2003) 045401. [arXiv:astro-ph/0303271](https://arxiv.org/abs/astro-ph/0303271), [doi:10.1103/PhysRevE.67.045401](https://doi.org/10.1103/PhysRevE.67.045401).

- [7] R. J. Protheroe, Effect of energy losses and interactions during diffusive shock acceleration: Applications to SNR, AGN and UHE cosmic rays, *Astropart. Phys.* 21 (2004) 415–431. [arXiv:astro-ph/0401523](#), [doi:10.1016/j.astropartphys.2004.02.004](#).
- [8] F. A. Aharonian, A. A. Belyanin, E. V. Derishev, V. V. Kocharovskiy, V. V. Kocharovskiy, Constraints on the extremely high-energy cosmic ray accelerators from classical electrodynamics, *Phys. Rev. D* 66 (2002) 023005. [arXiv:astro-ph/0202229](#), [doi:10.1103/PhysRevD.66.023005](#).
- [9] L. Landau, E. Lifshitz, *The classical theory of fields*, Addison–Wesley, 1951.
- [10] C. D. Dermer, G. Menon, *High energy radiation from black holes: Gamma rays, cosmic rays and neutrinos*, Princeton U. Pr., Princeton, USA, 2009.
- [11] S. Troitsky, Constraints on models of the origin of high-energy astrophysical neutrinos, *Usp. Fiz. Nauk* 191 (12) (2021) 1333–1360. [arXiv:2112.09611](#), [doi:10.3367/UFNe.2021.09.039062](#).
- [12] G. T. Zatsepin, V. A. Kuzmin, Upper limit of the spectrum of cosmic rays, *JETP Lett.* 4 (1966) 78–80.
- [13] F. W. Stecker, Effect of photomeson production by the universal radiation field on high-energy cosmic rays, *Phys. Rev. Lett.* 21 (1968) 1016–1018. [doi:10.1103/PhysRevLett.21.1016](#).
- [14] F. W. Stecker, Photodisintegration of ultrahigh-energy cosmic rays by the universal radiation field, *Phys. Rev.* 180 (1969) 1264–1266. [doi:10.1103/PhysRev.180.1264](#).
- [15] G. R. Blumenthal, Energy loss of high-energy cosmic rays in pair-producing collisions with ambient photons, *Phys. Rev. D* 1 (1970) 1596–1602. [doi:10.1103/PhysRevD.1.1596](#).
- [16] N. I. Shakura, R. A. Sunyaev, Black holes in binary systems. Observational appearance, *Astron. Astrophys.* 24 (1973) 337–355.
- [17] F. W. Stecker, C. Done, M. H. Salamon, P. Sommers, High-energy neutrinos from active galactic nuclei, *Phys. Rev. Lett.* 66 (1991) 2697–2700, [Erratum: *Phys.Rev.Lett.* 69, 2738 (1992)]. [doi:10.1103/PhysRevLett.66.2697](#).
- [18] O. Kalashev, D. Semikoz, I. Tkachev, Neutrinos in IceCube from active galactic nuclei, *J. Exp. Theor. Phys.* 120 (3) (2015) 541–548. [arXiv:1410.8124](#), [doi:10.1134/S106377611503022X](#).
- [19] C. W. Morgan, C. S. Kochanek, N. D. Morgan, E. E. Falco, The Quasar Accretion Disk Size – Black Hole Mass Relation, *Astrophys. J.* 712 (2010) 1129–1136. [arXiv:1002.4160](#), [doi:10.1088/0004-637X/712/2/1129](#).